Research Article | Vol. 10, No. 7 | 1 Jul 2019 | BIOMEDICAL OPTICS EXPRESS 3139
Biomedical Optics EXPRESS

Toward optimization of blood brain barrier opening induced by laser-activated perfluorocarbon nanodroplets

KRISTINA A. HALLAM[1,2] AND STANISLAV Y. EMELIANOV[1,2,*]

[1]*Wallace H. Coulter Department of Biomedical Engineering, Georgia Institute of Technology and Emory University School of Medicine, Atlanta, GA, USA*
[2]*School of Electrical and Computer Engineering, Georgia Institute of Technology, Atlanta, GA, USA*
**stas@gatech.edu*

Abstract: The blood brain barrier (BBB), a component of the brain's natural defense system, is often a roadblock for the monitoring and treatment of neurological disorders. Recently, we introduced a technique to open the blood brain barrier through the use of laser-activated perfluorohexane nanodroplets (PFHnDs), a phase-change nanoagent that undergoes repeated vaporization and recondensation when excited by a pulsed laser. Laser-activated PFHnDs were shown to enable noninvasive and localized opening of the BBB, allowing extravasation of various sized agents into the brain tissue. In this current work, the laser-activated PFHnD-induced BBB opening is further explored. In particular, laser fluence and the number of laser pulses used for the PFHnD-induced BBB opening are examined and evaluated both qualitatively and quantitatively to determine the effect of these parameters on BBB opening. The results of these studies show trends between increased laser fluence and an increased BBB opening as well as between an increased number of laser pulses and an increased BBB opening, however, with limitations on the extent of the BBB opening after a certain number of pulses. Overall, the results of these studies serve as a guideline to choosing suitable laser parameters for safe and effective BBB opening.

1. Introduction

A major challenge in the monitoring and treatment of various neurological diseases is the blood brain barrier (BBB) [1,2]. The BBB is a physiological barrier that prevents large molecules (>500 Da) in the vascular system from extravasating to the brain tissue [2,3]. Due to the selective nature of the BBB, delivery of contrast agents or therapeutics is greatly hindered, making it difficult to monitor and treat neurological diseases [1,2,4–6]. To overcome the BBB, various methods, such as surgical resection, device implantation, and chemical manipulation of the tissue are currently used [3,4]. However, there are inherent risks with these methods including invasiveness and widespread opening of the BBB, increasing the potential for infection and resulting in limited success for treating diseases such as brain cancers, Alzheimer's, and Huntington's [1,7]. Thus, the focus for monitoring and treatment of neurological diseases in the brain has shifted towards noninvasive measures, where BBB opening can be performed transiently, locally, and repeatedly [2,5].

One well-developed, noninvasive method of opening the BBB is microbubble-assisted focused ultrasound (FUS) [2,5,8]. This method relies on the interaction of a focused ultrasound field and oscillating microbubbles to stretch endothelial tight junctions and increase uptake through mechanotransduction pathways, allowing larger molecules to extravasate [2,9,10]. Microbubble-assisted FUS for BBB opening is a technique that has been evaluated for safety and efficacy [5,11–13]. FUS frequency, pulse duration, PRF, and pressure amplitude, as well as microbubble composition and dose have been examined to determine the optimal range of parameters [14–22]. Consequently, this technology is used in applications ranging from small animal studies to clinical trials [23,24].

#360612 https://doi.org/10.1364/BOE.10.003139
Journal © 2019 Received 4 Mar 2019; revised 30 May 2019; accepted 30 May 2019; published 6 Jun 2019

Biomedical Optics EXPRESS

Recently, perfluorocarbon nanodroplets (PFCnDs), a descendant of microbubbles, have been investigated as a means to transiently open the BBB [25–27]. PFCnDs are a phase-change nanoagent capable of changing from liquid nanodroplet to gas microbubble when activated via acoustic or electromagnetic energy [28–30]. PFCnDs are comprised of a shell, perfluorocarbon core, and an optical trigger when activated via an optical energy source [29]. Specifically, laser-activated PFCnDs rely on the interaction between a pulsed laser and an optical trigger within the droplet to induce the phase change from liquid to gas [29]. Because perfluorocarbon itself is not optically absorbing, a highly optically absorbing dye or nanoparticle is encapsulated within the PFCnD to enable PFCnD vaporization. Phase-change of the PFCnD occurs due to the localized heating and photoacoustic pressure wave that result from the optical trigger-laser interaction [29]. For laser-activated PFCnD induced BBB opening, we investigated perfluorohexane nanodroplets (PFHnDs) [27]. PFHnDs are attractive for use in BBB opening due to their ability to undergo repeated phase-change from liquid to gas [31–34], creating an oscillatory-like behavior and allowing laser-activated PFHnDs multiple opportunities to interact with the BBB and enable opening.

In addition to enabling BBB opening, laser-activated PFCnDs are also capable of providing localized ultrasound (US) and photoacoustic (PA) image contrast [28,35–38]. The phase-change of PFCnDs from liquid nanodroplet to gas microbubble provides US contrast while the pulsed laser-optical trigger interaction that initiates the phase-change produces PA contrast. The unique US/PA image contrast provided by laser-activated PFCnDs allows for use in various *in vivo* applications from super resolution imaging to multiplexed imaging [32,33,37,39]. Further, PFCnDs are capable of carrying cargo within the droplet or on the shell, making them attractive as controlled release delivery vehicles [40]. Their nanometer size also makes PFCnDs capable of extravasation across barriers such as leaky vasculature within a tumor or an opened BBB [27,40–42]. As a result, the versatile nature of PFCnDs shows their potential to be utilized in a wide variety of applications including the central nervous system.

To understand fully the capabilities of laser-activated PFCnDs in BBB opening and in neurological applications, it is necessary to study the effects of the laser parameters used to activate the PFCnDs. In these studies, we focus on two particular parameters, laser fluence and number of laser pulses used, with the results demonstrating how BBB opening can be controlled via laser-activated PFCnDs.

2. Materials and methods

2.1 Synthesis and characterization of IR-1048 laser-activated perfluorohexane nanodroplets (PFHnDs)

IR-1048 perfluorohexane nanodroplets (PFHnDs) were synthesized using IR-1048 dye (Sigma-Aldrich), perfluorohexane (PFH, FluoroMed, L.P.), and a lipid shell composed of 1,2-distearoyl-sn-glycero-3-phosphoethanolamine-N-[amino(polyethylene glycol)-2000] (DSPE-PEG(2000), 25 mg/mL, Avanti Polar Lipids, Inc.) and 1,2-distearoyl-sn-glycero-3-phosphocholine (18:0 PC (DSPC), 25 mg/mL, Avanti Polar Lipids). To create the lipid shell, 40 µL of DSPE-PEG(2000) and 8 µL of 18:0 PC (DSPC) were added to a 10 mL pear-shaped flask (Sigma-Aldrich). An IR-1048 dye solution was prepared in chloroform (1mg/mL), and 200 µL was added to the flask. An additional 1 mL of chloroform was added to the flask to enable a smooth lipid cake. A rotary evaporator (Rotovapor, Büchi) was used at reduced pressure to remove the chloroform from the flask leaving an IR-1048 dye-coated lipid cake. The lipid cake was resuspended in 1 mL of PBS using a water bath sonicator (VWR, 180W). The solution was placed in a 7 mL scintillation vial, and 150 µL of PFH was added. The vial was vortexed for 10 seconds (Vortex Mixer, Fisher Scientific) and sonicated for five minutes in an ice-cold water bath (VWR, 180 W). The PFHnD solution was transferred to a 2 mL centrifuge tube and centrifuged for 60 seconds in a mini-centrifuge (Mini-Spin, Eppendorf) to remove excess PFH and IR-1048 dye. The supernatant was transferred to a new 2 mL

Biomedical Optics EXPRESS

centrifuge tube, and the pellet was discarded. Prior to *in vivo* experiments, droplets were left under UV light for 30 minutes for sterilization.

PFHnD size and zeta potential were measured in PBS (pH 7.4) using a dynamic light scattering instrument (Zetasizer Nano ZS, Malvern Instruments Ltd.). To generate the absorbance spectra of IR-1048 PFHnDs, a spectrophotometer was used to measure IR-1048 PFHnDs and blank PFHnDs, i.e. PFHnDs synthesized as described above without dye. The blank PFHnD spectra was then subtracted from the IR-1048 PFHnD spectra. PFHnD concentration measurements were made using a NanoSight NS300 (Malvern Instruments Ltd.).

2.2 In vivo laser-activated PFHnD induced blood brain barrier opening

All animal studies were conducted under the protocol approved by the Institutional Animal Care and Use Committee at Georgia Institute of Technology. Animal studies were performed as described previously [27]. Briefly, an injection of sustained released buprenorphine (IP, 0.8 mg/kg) was administered to each animal (Balb/c mouse, Jax), prior to anesthesia. Mice were anesthetized using a combination of isoflurane (2%, Henry Schein) and medical air (0.6 L/min, Airgas). Mice were positioned in a stereotax in the prone position, on a heating pad (Stoelting Co). Hair from the scalp was removed through shaving and depilatory cream. Proparacaine (0.5%, Henry Schein) was applied to the eyes, and a retro-orbital injection of 50 µL of 3% w/v sterile filtered Evans Blue (EB) (Sigma Aldrich) was administered with a co-injection of 70 µL of IR-1048 PFHnDs (~10^8 droplets). To allow for irradiation of the right side of the brain, animals were positioned underneath an unfocused 1.5 mm core diameter optical fiber (0.39 NA, Thorlabs, Inc.). Irradiation was performed with a Vibrant laser (10 Hz, 5-7 ns pulse length, Opotek Inc.) at a wavelength of 1064 nm.

Six animal groups (n = 3 mice) were treated with a varying number of laser pulses and varying laser fluences. Three animal groups were exposed to a fluence of 56 mJ/cm^2, with the number of laser pulses being 300, 600, or 1200 pulses. As the PRF of the laser used was 10 Hz, the total laser irradiation time for these three groups was 30, 60, and 120 seconds, respectively. Two additional animal groups were exposed to 600 laser pulses and had laser fluences of 38 or 70 mJ/cm^2. The sixth group of animals acted as a control group, with no laser irradiation or a co-injection. Other controls of co-injection only or laser irradiation only have been performed previously and showed no BBB opening effect, so the control here serves a baseline for the experimental groups [27]. After laser irradiation, mice were allowed to recover, with no gross behavioral damage observed. After four hours, animals were euthanized via an IP Euthatal injection (150 mg/kg) followed by perfusion with 1X PBS (pH 6.8) and 4% paraformaldehyde (PFA). Heads were removed and post-fixed overnight in 4% PFA solution. After 24 hours, brains were excised, and whole brain photographs were taken.

2.3 Ex vivo ultrasound and photoacoustic imaging

Brains, excised and fixed, were placed on top of an 8% gelatin base in a container filled with degassed water. Samples were imaged using an ultrasound and photoacoustic (US/PA) imaging system (Vevo LAZR, FUJIFILM VisualSonics Inc.) with a 40 MHz ultrasound and photoacoustic imaging probe (LZ-550, FUJIFILM VisualSonics Inc.). The US/PA imaging system's tunable Nd:YAG laser (20 Hz, 5-7 ns pulse length) was operated at a wavelength of 1064 nm and a fluence of 12-14 mJ/cm^2. Brains were imaged at an US/PA frame rate of 5 frames per second. Coronal and sagittal 3D US/PA images were collected with a distance step size of 0.102 mm for a total of about 14 mm and 12 mm, respectively. US/PA imaging was performed for all six animal groups.

2.4 Ultrasound and photoacoustic image processing

Coronal ultrasound and photoacoustic image sets were processed in MATLAB (Mathworks, Inc.). US/PA images were thresholded to reduce noise and exported to generate 3D whole

Biomedical Optics EXPRESS

brain images using AMIRA (Thermo Scientific). Top view and corner cut images of the treated (right) side of the brain, viewed from behind the cerebellum, were captured using AMIRA.

To determine the photoacoustic volume from IR-1048 dye for each brain, the photoacoustic data set for each coronal image was co-registered with its respective ultrasound data set, and any PA signal located outside of the co-registered US coronal section was removed. The treated (right side) PA signal area of each coronal section was determined based on the location of the PA signal within the image. Outliers from the location data set were removed as to eliminate any PA signal from the untreated (left) side of the brain that could have resulted from other sources, such as deoxygenated hemoglobin remaining within the vasculature post-perfusion. The area of PA signal was calculated by multiplying the total width and depth of the PA location data set in the image. After the area was calculated for each coronal image, volume was calculated by totaling the PA area for each brain and multiplying by the coronal image step size of 0.102 mm.

2.5 Histology and immunohistochemistry

After 3D US/PA imaging, brains were transferred to a solution of 30% sucrose and stored at 4°C for five days. Brains were snap frozen, and 20 µm coronal sections were cut using a cryostat (Leica CM 1860, Leica Biosystems). For each brain, 48-60 sections were cut and analyzed, spanning a total region of 0.96-1.2 mm within the brain. Standard hematoxylin (Gill No. 2, Sigma-Aldrich) and eosin (VWR) (H&E) was performed. H&E pictomicrographs were captured using the bright field mode of a Zeiss AxioObserver Z1 Microscope. Immunohistochemistry (IHC) was also performed using a secondary antibody of goat anti-mouse immunoglobulin G (H + L) tagged with Alexa Fluor 488 (Invitrogen) and 4',6-diamidino-2-phenylindole (DAPI, Invitrogen). IHC pictomicrographs were captured with a Zeiss Laser Scanning Confocal Microscope 700.

Zen lite software (Zeiss) was used to evaluate the fluorescence area of the IHC pictomicrographs of each animal. Fluorescence area was calculated using the profile view in the Zen lite software. Using a rectangular profile, IgG fluorescence signal was displayed across each coronal slice and thresholded to remove background noise. The area of IgG fluorescence was then calculated based on the location of above-threshold fluorescence.

3. Results

3.1 Characterization of IR-1048 laser-activated PFHnDs

Lipid shelled, IR-1048 perfluorohexane nanodroplets (PFHnDs) were characterized by size, charge, and UV-VIS-NIR absorbance as shown below (Fig. 1). PFHnDs had an average diameter of 265 ± 64.7 nm and a charge of −5.2 ± 4.4 mV in PBS (pH 7.4) (Figs. 1(A) and 1(B)). When activated, PFHnDs are expected to expand to 1.25 µm (5X their nanodroplet diameter), putting theses activated droplets in the size range of microbubbles used for FUS BBB opening [2,30]. Optical absorbance spectra measured for IR-1048 PFHnDs shows a peak optical absorption near 1064 nm, the wavelength used for laser-activation of PFHnDs (Fig. 1(C)). Irradiation at 1064 nm allows for increased light penetration in tissue, enabling activation of PFHnDs at increased depths [29,43]. Evans Blue (EB), the dye co-administered with PFHnDs in *in vivo* experiments to qualitatively and macroscopically evaluate BBB opening, has a peak optical absorption near 600 nm and minimal absorption at 1064 nm. As a result, EB will not interact with the 1064 nm laser light used for laser-activated PFHnD BBB opening and *ex vivo* imaging.

Biomedical Optics EXPRESS

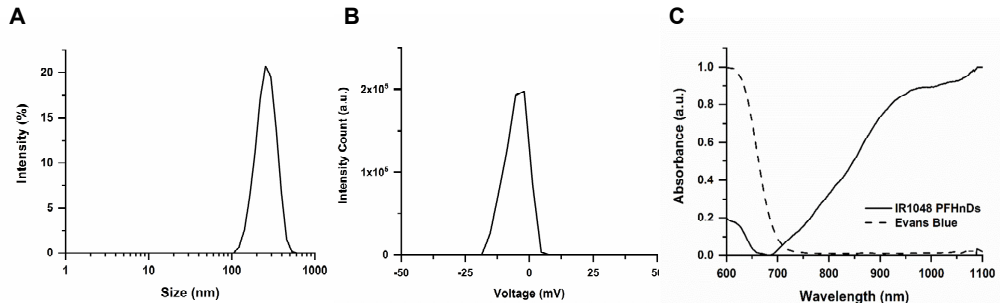

Fig. 1. Characterization of IR-1048 perfluorohexane nanodroplets (PFHnDs). (A) IR-1048 PFHnD size distribution, 265 ± 64.7 nm. (B) Zeta potential of IR-1048 PFHnDs, −5.2 ± 4.4 mV. (C) Normalized absorbance spectra of IR-1048 PFHnDs with a peak optical absorption near 1064 nm and Evans Blue dye with a peak optical absorption near 600 nm. Both IR-1048 PFHnDs and Evans Blue are used for *in vivo* blood brain barrier opening experiments.

3.2 Evans Blue extravasation and histological analysis of laser-activated PFHnD induced blood brain barrier opening

Evans Blue extravasation and hematoxylin and eosin (H&E) staining was compared for each animal group based on the number of laser pulses used (Fig. 2). EB extravasation provides a macroscopic view of BBB opening, and H&E staining evaluates the tissue for damage, with red blood cells (RBCs) in the tissue indicating microhemorrhages [21]. For 0 laser pulses, i.e. no laser irradiation, no EB extravasation was visible nor was there any abnormalities in the stained tissue (Fig. 2(A)). At 300 laser pulses, EB extravasation is visible in the top-view photograph and coronal cross-section photograph, as indicated by the white, dashed oval, outlining the EB extravasation area (Fig. 2(B)). H&E staining shows no differences between the treated (right) and untreated (left) sides of the brain (Fig. 2(B)). When 600 laser pulses are used, EB extravasation is evident, and H&E staining shows some RBC extravasation, denoted by the bright red staining in the tissue slice (Fig. 2(C)). With 1200 laser pulses, EB extravasation is also apparent in both the top view and coronal cross-section images (Fig. 2(D)). However, in this group, RBC extravasation was not found, and both treated (right) and untreated (left) tissue were the same (Fig. 2(D)). As the number of laser pulses increases from 300 to 600, there is an increase in EB extravasation in both the top view and coronal cross-section photographs (Figs. 2(B) and 2(C)). From 600 to 1200 laser pulses, there appears to be a similar EB extravasation footprint from the top view photographs, however, there is an increase in the area of EB extravasation in the coronal cross-section images from 600 to 1200 laser pulses (Figs. 2(C) and 2(D)).

Varying laser fluences were also evaluated for their effect on EB extravasation and H&E staining (Fig. 3). As was shown in with 0 laser pulses, a fluence of 0 mJ/cm^2 (no laser irradiation) shows no EB extravasation or tissue abnormalities (Figs. 2(A) and 3(A)). When the laser fluence is increased to 38 mJ/cm^2, EB extravasation is evident, in both the top view photograph and coronal cross-section photograph, where the EB extravasation of the coronal cross-section is outlined by a white, dashed oval (Fig. 3(B)). H&E staining shows no differences between the treated and untreated sides of the brain (Fig. 3(B)). In the case of 56 mJ/cm^2, EB extravasation is widespread on the treated side of the brain, and RBC extravasation on the treated side is seen in H&E staining (Figs. 2(C) and 3(C)). At 70 mJ/cm^2, EB extravasation occurs, and the treated side of the brain shows RBC extravasation (Fig. 3(D)). By increasing laser fluence, EB extravasation spread increases, and at higher fluences, RBC extravasation is present (Figs. 3(B) and 3(D)).

Biomedical Optics EXPRESS

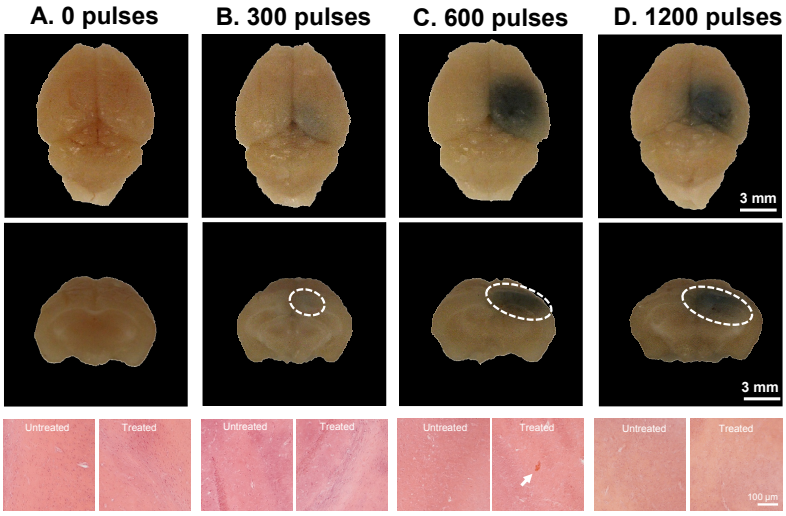

Fig. 2. Representative Evans Blue (EB) dye extravasation top view and cross-sectional photographs and hemotoxalyin & eosin (H&E) pictomicrographs for varying number of laser pulses. EB dye extravasation is outlined on the coronal cross-section with a white, dashed oval. H&E pictomicrographs are shown for both treated (right) and untreated (left) sides of the brain, with presence of red blood cells indicated by a white arrow and bright red staining within the tissue. Number of laser pulses includes (A) 0 laser pulses, (B) 300 laser pulses, (C) 600 laser pulses, and (D) 1200 laser pulses. Note: Laser pulse in A and C use the same images as laser fluence Figs. 3(A) and 3(C), and experiments shown in B–D were performed at a laser fluence of 56 mJ/cm^2.

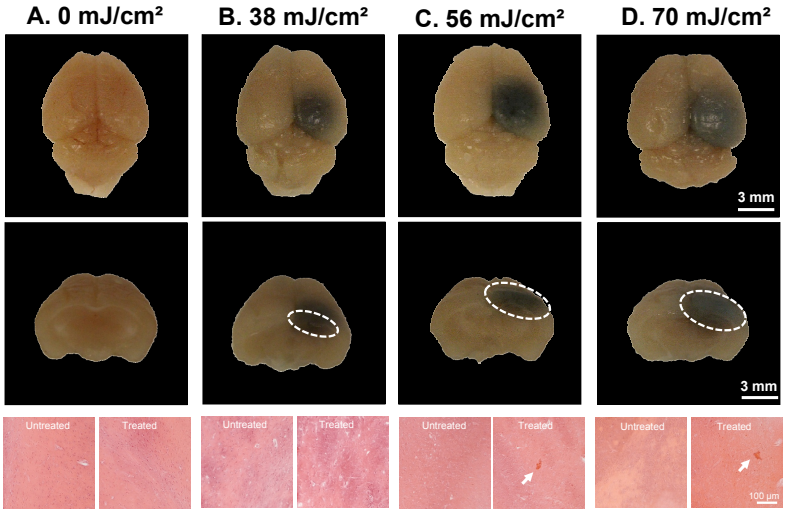

Fig. 3. Representative Evans Blue (EB) dye extravasation top view and cross-sectional photographs and hemotoxalyin & eosin (H&E) pictomicrographs for varying laser fluences. EB dye extravasation is outlined on the coronal cross-section with a white, dashed oval. H&E pictomicrographs are shown for both treated (right) and untreated (left) sides of the brain, with presence of red blood cells indicated by a white arrow and bright red staining within the tissue. Laser fluences include (A) 0 mJ/cm^2, (B) 38 mJ/cm^2, (C) 56 mJ/cm^2, and (D) 70 mJ/cm^2. Note: Laser fluence A and C use the same images as laser pulse Figs. 2(A) and 2(C), and experiments shown in B–D were performed with 600 laser pulses.

In addition to H&E staining, immunohistochemistry was performed to examine the extravasation of the secondary antibody mouse immunoglobulin G (IgG). Mouse IgG has a molecular weight of 150 kDa and will not extravasate unless the BBB is opened, as the

Biomedical Optics EXPRESS

molecular weight limit for the BBB is 500 Da [3,44]. As can be seen with the whole brain, coronal section and magnified confocal pictomicrographs of the 0 laser pulses/ 0 mJ/cm^2 (no laser) case, fluorescence from DAPI is present, but there is minimal fluorescence signal from IgG (Figs. 4(A) and 4(B)). Minimal fluorescence from IgG is seen in the untreated (left) side of the brain for all laser pulse and laser fluence variations (Figs. 4(A), 4(C), 4(E), 4(G), 4(I), and 4(K)). In the animal groups where irradiation occurs, IgG fluorescence is visible throughout the treated (right side) region (Figs. 4(D), 4(F), 4(H), 4(J), and 4(L)). When the number of laser pulses is varied, fluorescent intensity from 0 laser pulses to 600 laser pulses increases (Figs. 4(B), 4(F), amd 4(H)), but from 600 to 1200 laser pulses, the fluorescence signal does not seem to change (Figs. 4(H) and 4(J)). A similar trend is observed for increasing laser fluence where fluorescence increases on the treated side from 0 mJ/cm^2 to 56 mJ/cm^2 and remains constant from 56 to 70 mJ/cm^2 (Figs. 4(B), 4(D), 4(H), and 4(L)).

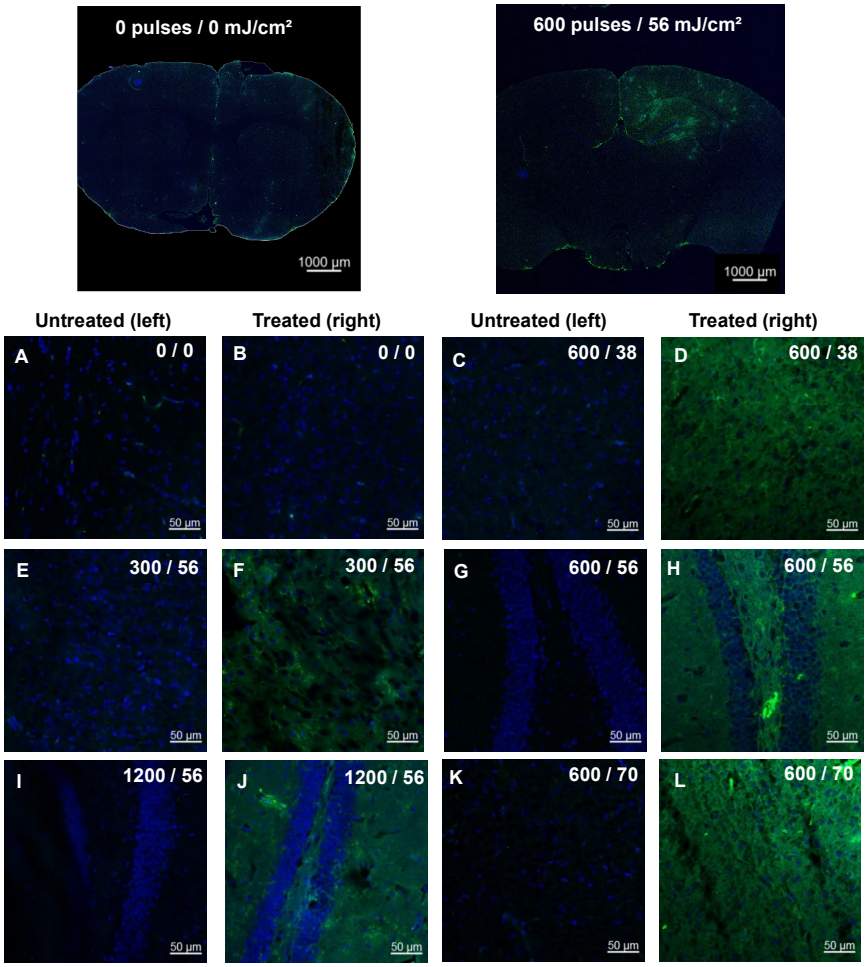

Fig. 4. Immunohistochemistry staining for secondary antibody IgG and DAPI. The coronal sections displayed are representative images of overall IgG (green) and DAPI (blue) fluorescence while the magnified images display the difference in IgG fluorescence between the untreated (left) and treated (right) sides. Magnified images are labeled as number of laser pulses/laser fluence (mJ/cm^2).

3.3 Ultrasound and photoacoustic analysis of IR-1048 dye extravasation

Ex vivo ultrasound and photoacoustic (US/PA) imaging was performed, and 3D whole brain images were reconstructed to evaluate the volume of extravasated IR-1048 dye. This NIR

Biomedical Optics EXPRESS

absorbing dye is contained within the PFHnDs; however, when laser-activated PFHnD BBB opening occurs, dye is able to extravasate across the BBB and produces a PA signal when imaged at its peak wavelength [27]. Reconstructed 3D US images are displayed in grayscale, and the reconstructed 3D PA signal is displayed using a hot colormap (Fig. 5). At 0 pulses (no laser), there is minimal, background PA signal present, but as the number of laser pulses increases from 300 to 1200 pulses, the volume of PA signal within the brain can be seen to increase in the treated (right side) of the brain.

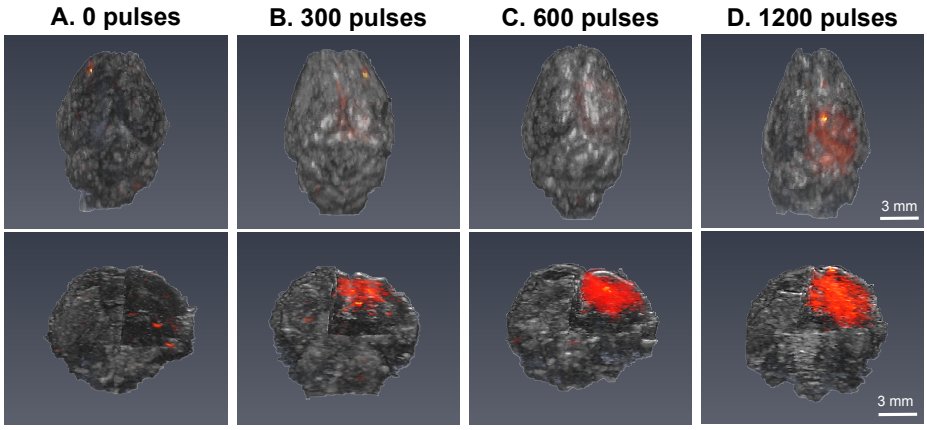

Fig. 5. Reconstructed 3D top view and right side, corner cut images of ultrasound (US, grayscale) and photoacoustic (PA, hot colormap) data for varying number of laser pulses: (A) 0 pulses, (B) 300 pulses, (C) 600 pulses, and (D) 1200 pulses. Note: Laser pulse A and C use the same images as laser fluence Figs. 6(A) and 6(C), and experiments shown in B–D were performed with a laser fluence of 56 mJ/cm^2.

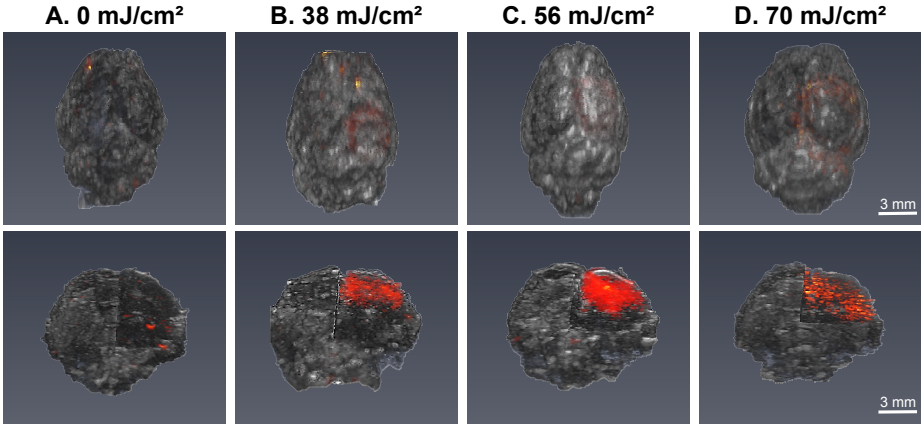

Fig. 6. Reconstructed 3D top view and right side, corner cut images of ultrasound (US, grayscale) and photoacoustic (PA, hot colormap) data for varying laser fluences: (A) 0 mJ/cm^2, (B) 38 mJ/cm^2, (C) 56 mJ/cm^2, and (D) 70 mJ/cm^2. Note: Laser fluence A and C use the same images as laser pulse Figs. 5(A) and 5(C), and experiments shown in B–D were performed with 600 laser pulses.

The trend in PA signal volume can also be examined as laser fluence is varied (Fig. 6). At 0 mJ/cm^2 (no laser), there is minimal signal, and as laser energy increases from 38 mJ/cm^2 to 70 mJ/cm^2, the PA signal volume increases. Although the volume of PA signal at 70 mJ/cm^2 is increased, the overall PA signal intensity appears to be lower than the intensity at 56 mJ/cm^2 (Figs. 6(C) and 6(D)).

Biomedical Optics EXPRESS

3.4 Quantitative fluorescence and photoacoustic analysis

Quantitative analysis of fluorescence signal from IgG and PA signal from IR-1048 dye was completed for the five animal groups where laser irradiation was performed (Fig. 7). The fluorescence area and PA volume were not calculated for the no laser (0 laser pulses, 0 mJ/cm^2) case, as there is no calculable fluorescence area or PA volume for this animal group. Examining the number of laser pulses from 300 to 600 pulses, there is an increase in fluorescence area (Fig. 7(A)). However, fluorescence area measurements from 600 to 1200 pulses are similar in mean and median, potentially indicating a saturation point with regards to the area over which of IgG is delivered to the tissue as the number of laser pulses increases. When the laser fluence is increased, the fluorescence area also increases (Fig. 7(B)). With PA volume measurements, similar trends are seen (Figs. 7(C) and 7(D)). There is an increase in PA volume as the number laser pulses increases from 300 to 600 pulses, but there is not an increase when comparing 600 to 1200 laser pulses. As the laser fluence is increased from 38 mJ/cm^2 to 56 mJ/cm^2 to 70 mJ/cm^2, the PA volume increases.

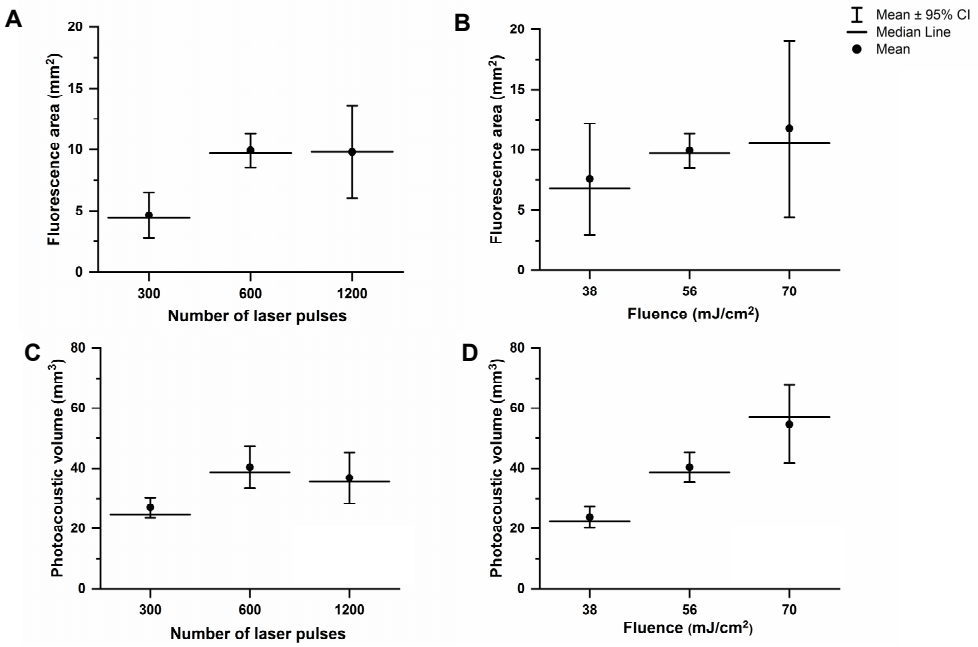

Fig. 7. Quantitative evaluation of fluorescence area and photoacoustic volume for the varying number of laser pulses and laser fluences used. (A) Fluorescence area vs. number of laser pulses for 300, 600, and 1200 pulses. (B) Fluorescence area vs. fluence for 38, 56, and 70 mJ/cm^2. (C) Photoacoustic volume vs. number of laser pulses for 300, 600, and 1200 laser pulses. (D) Photoacoustic volume for 38, 56, and 70 mJ/cm^2. The circle marker indicates the mean value calculated for each animal group. The horizontal line identifies the median, and the vertical line marked with crossbars identifies the 95% confidence interval.

4. Discussion

Through the variation of a range of laser fluences and laser pulses, the extent of laser-activated perfluorohexane nanodroplet (PFHnD) induced blood brain barrier (BBB) opening was controlled. BBB opening was evaluated through Evans Blue (EB) staining of the tissue, fluorescence produced by the secondary antibody IgG, and photoacoustic (PA) signal produced by IR-1048 dye (Figs. 2–6). Damage to the tissue indicated by RBC extravasation was also evaluated to determine which range of laser fluences and laser pulses was safe (Figs. 2 and 3). Overall, it was seen that extent of BBB opening increased with increased laser

Biomedical Optics EXPRESS

fluence (Figs. 7(B) and 7(D)). When the number of laser pulses was increased from 300 to 600 pulses, there was an increase in fluorescence area and PA volume (Figs. 7(A) and 7(C)). However, the trend in BBB opening remained constant when the number of laser pulses was increased from 600 to 1200. The results of these studies show how BBB opening can be modulated through the choice of laser parameters used for activation of PFHnDs.

The increased extent of BBB opening for increased laser fluence used is expected. Due to the optical properties of tissue, the ability of light to penetrate tissue and vaporize the droplets is in part dependent on the amount of laser fluence used [43]. Therefore, an increased laser fluence used in laser-activated PFHnD induced BBB opening can result in increased depth penetration, and this increased fluence will likely activate more PFHnDs, causing BBB opening in a larger volume within the tissue. This tissue-fluence interaction may also explain the trend seen when the number of laser pulses is increased. Although an increased number of pulses will allow for an increased number of PFHnD droplet phase-changes or oscillations, which may help to increase BBB opening, the laser fluence footprint is expected to be the same when the same fluence is used. As a result, there is likely to be a limit to the extent of BBB opening when the same fluence is used but the number of laser pulses is increased.

Furthermore, it is important to note that there were some cases where red blood cell extravasation occurred. When 56 mJ/cm^2 and 600 laser pulses were used, RBC extravasation was apparent in the tissue (Figs. 2(C) and 3(C)). In addition, at 70 mJ/cm^2 and 600 laser pulses, RBC extravasation was visible (Fig. 3(D)). Thus, choosing lower fluences may be optimal to enable effective BBB opening without damage to the tissue. Interestingly, at 1200 laser pulses and a fluence of 56 mJ/cm^2, RBC extravasation was not seen (Fig. 2(D)). There are a few possibilities as to why 1200 pulses did not show damage, such as variation per animal or slight differences in the PFCnD size distribution synthesized for each set of experiments. However, the trends seen in Evans Blue extravasation, IgG fluorescence, and IR-1048 dye delivery show that these slight differences have not affected the outcome of BBB opening, suggesting that damage should be seen in the 1200 laser pulse group (Figs. 2(D), 4(I), 4(J), and 5(D)). As a result, the upper limit or guideline for safe, laser-activated PFHnD induced BBB opening given these experiments should be the lowest laser fluence and laser pulse number to show RBC extravasation, which is 56 mJ/cm^2 and 600 laser pulses.

Other parameters can also be explored to optimize laser-activated PFCnD induced BBB opening. With regard to laser parameters, the laser pulse repetition frequency (PRF) could be modified. In these studies, a laser PRF of 10 Hz was used. A lower PRF would increase the time between phase-change events, potentially reducing the concentration of phase-changing PFHnDs within the laser irradiated volume which may help to reduce tissue damage seen at higher fluences. Laser irradiation wavelength could also be adjusted. The current wavelength of 1064 nm used was selected for increased depth penetration into tissue, but other NIR absorbing wavelengths could be used. Regardless, effectiveness and extent of BBB opening would be dependent upon the peak absorption wavelength of the optical trigger within PFCnDs, so wavelength used should coincide with the optical trigger. PFCnD parameters would also affect BBB opening [25,26], similar to how microbubbles affect BBB opening [14,17,18,22]. Parameters such as PFCnD size, concentration, perfluorocarbon core, and encapsulated optical trigger can also affect the safety and efficacy of laser-activated PFHnD induced BBB opening. Overall, these studies focused on laser fluence and laser pulses used and provide a guideline to how PFCnD BBB opening can be controlled through laser irradiation. Nevertheless, there is still space to improve upon laser-activated PFCnD BBB opening, primarily through exploration of PFCnD parameters.

A fully optimized laser-activated PFCnD induced BBB opening would allow laser-activated PFCnDs to act in multiple roles in the monitoring and treatment of neurological diseases. US/PA imaging of extravasated photoacoustic contrast in the brain *in vivo* has been established [45,46], and therefore PFCnDs could contribute to not only BBB opening but also US/PA contrast within the brain. Contrast provided via laser-activated PFCnDs could enable

Biomedical Optics EXPRESS

monitoring of BBB opening as well as well as monitoring of the delivery of any cargo, therapeutic or diagnostic, contained within PFCnDs. In addition, laser-activated PFCnD induced BBB opening would allow for delivery of other PA contrast agents, possibly furthering the capabilities of longitudinal or multiplexed US/PA imaging within the brain. Altogether, laser-activated PFCnD induced BBB opening and the versatility of PFCnDs have the potential to play a significant role in US/PA imaging and therapy in the central nervous system.

5. Conclusion

The results of these studies show how laser-activated perfluorohexane nanodroplet (PFHnD) induced blood brain barrier (BBB) opening can be controlled by adjusting both laser fluence and the number of laser pulses used. An increased laser fluence increases the volume of BBB opening, as does increasing the number of pulses used. However, there appears to be a limit to the extent of BBB opening when increasing the number of laser pulses, as the difference in BBB opening after a certain number of pulses was minimal. Furthermore, at higher fluences and with increased laser pulses, red blood cell extravasation is visible. To enable safe and effective BBB opening, laser parameters must be appropriately chosen, and these studies provide guidelines toward optimized laser-activated PFHnD BBB opening. As a result, laser-activated PFHnDs have the potential to safely and effectively deliver various sized agents across the BBB, enabling real-time monitoring and treatment of neurological diseases.

Funding

National Institutes of Health (NIH) (NS102860).

Acknowledgements

The authors would like to thank Davis Palmie of Georgia Institute of Technology for his help with cryosectioning and Andrew Zhao of Georgia Institute of Technology for his helpful comments and discussion. K.A.H. would wishes to acknowledge J. Norman and Rosalyn Wells for their fellowship support. We also wish to acknowledge the core facilities at the Parker H. Petit Institute for Bioengineering and Bioscience at the Georgia Institute of Technology for the use of their shared equipment, services, and expertise.

Disclosures

The authors declare that there are no conflicts of interest related to this article.

References

1. W. M. Pardridge, "The blood-brain barrier: bottleneck in brain drug development," NeuroRx **2**(1), 3–14 (2005).
2. C. Poon, D. McMahon, and K. Hynynen, "Noninvasive and targeted delivery of therapeutics to the brain using focused ultrasound," Neuropharmacology **120**, 20–37 (2017).
3. M. Aryal, C. D. Arvanitis, P. M. Alexander, and N. McDannold, "Ultrasound-mediated blood-brain barrier disruption for targeted drug delivery in the central nervous system," Adv. Drug Deliv. Rev. **72**, 94–109 (2014).
4. N. Vykhodtseva, N. McDannold, and K. Hynynen, "Progress and problems in the application of focused ultrasound for blood-brain barrier disruption," Ultrasonics **48**(4), 279–296 (2008).
5. E. E. Konofagou, "Optimization of the ultrasound-induced blood-brain barrier opening," Theranostics **2**(12), 1223–1237 (2012).
6. U. Tosi, C. S. Marnell, R. Chang, W. C. Cho, R. Ting, U. B. Maachani, and M. M. Souweidane, "Advances in Molecular Imaging of Locally Delivered Targeted Therapeutics for Central Nervous System Tumors," Int. J. Mol. Sci. **18**(2), 351 (2017).
7. T. D. Azad, J. Pan, I. D. Connolly, A. Remington, C. M. Wilson, and G. A. Grant, "Therapeutic strategies to improve drug delivery across the blood-brain barrier," Neurosurg. Focus **38**(3), E9 (2015).
8. K. Hynynen, N. McDannold, N. Vykhodtseva, and F. A. Jolesz, "Non-invasive opening of BBB by focused ultrasound," Acta Neurochir. Suppl. (Wien) **86**, 555–558 (2003).
9. Y. S. Tung, F. Vlachos, J. A. Feshitan, M. A. Borden, and E. E. Konofagou, "The mechanism of interaction between focused ultrasound and microbubbles in blood-brain barrier opening in mice," J. Acoust. Soc. Am. **130**(5), 3059–3067 (2011).

Biomedical Optics EXPRESS

10. N. Sheikov, N. McDannold, N. Vykhodtseva, F. Jolesz, and K. Hynynen, "Cellular mechanisms of the blood-brain barrier opening induced by ultrasound in presence of microbubbles," Ultrasound Med. Biol. **30**(7), 979–989 (2004).
11. J. Shin, C. Kong, J. S. Cho, J. Lee, C. S. Koh, M. S. Yoon, Y. C. Na, W. S. Chang, and J. W. Chang, "Focused ultrasound-mediated noninvasive blood-brain barrier modulation: preclinical examination of efficacy and safety in various sonication parameters," Neurosurg. Focus **44**(2), E15 (2018).
12. T. Kobus, N. Vykhodtseva, M. Pilatou, Y. Zhang, and N. McDannold, "Safety Validation of Repeated Blood-Brain Barrier Disruption Using Focused Ultrasound," Ultrasound Med. Biol. **42**(2), 481–492 (2016).
13. J. H. Hwang, J. Tu, A. A. Brayman, T. J. Matula, and L. A. Crum, "Correlation between inertial cavitation dose and endothelial cell damage in vivo," Ultrasound Med. Biol. **32**(10), 1611–1619 (2006).
14. G. Samiotaki, F. Vlachos, Y. S. Tung, and E. E. Konofagou, "A quantitative pressure and microbubble-size dependence study of focused ultrasound-induced blood-brain barrier opening reversibility in vivo using MRI," Magn. Reson. Med. **67**(3), 769–777 (2012).
15. H. Chen and E. E. Konofagou, "The size of blood-brain barrier opening induced by focused ultrasound is dictated by the acoustic pressure," J. Cereb. Blood Flow Metab. **34**(7), 1197–1204 (2014).
16. J. J. Choi, M. Pernot, S. A. Small, and E. E. Konofagou, "Noninvasive, transcranial and localized opening of the blood-brain barrier using focused ultrasound in mice," Ultrasound Med. Biol. **33**(1), 95–104 (2007).
17. J. J. Choi, J. A. Feshitan, B. Baseri, S. Wang, Y. S. Tung, M. A. Borden, and E. E. Konofagou, "Microbubble-size dependence of focused ultrasound-induced blood-brain barrier opening in mice in vivo," IEEE Trans. Biomed. Eng. **57**(1), 145–154 (2010).
18. N. McDannold, N. Vykhodtseva, and K. Hynynen, "Blood-brain barrier disruption induced by focused ultrasound and circulating preformed microbubbles appears to be characterized by the mechanical index," Ultrasound Med. Biol. **34**(5), 834–840 (2008).
19. M. A. O'Reilly, A. C. Waspe, M. Ganguly, and K. Hynynen, "Focused-ultrasound disruption of the blood-brain barrier using closely-timed short pulses: influence of sonication parameters and injection rate," Ultrasound Med. Biol. **37**(4), 587–594 (2011).
20. N. McDannold, N. Vykhodtseva, and K. Hynynen, "Effects of acoustic parameters and ultrasound contrast agent dose on focused-ultrasound induced blood-brain barrier disruption," Ultrasound Med. Biol. **34**(6), 930–937 (2008).
21. R. Chopra, N. Vykhodtseva, and K. Hynynen, "Influence of exposure time and pressure amplitude on blood-brain-barrier opening using transcranial ultrasound exposures," ACS Chem. Neurosci. **1**(5), 391–398 (2010).
22. C. Bing, Y. Hong, C. Hernandez, M. Rich, B. Cheng, I. Munaweera, D. Szczepanski, Y. Xi, M. Bolding, A. Exner, and R. Chopra, "Characterization of different bubble formulations for blood-brain barrier opening using a focused ultrasound system with acoustic feedback control," Sci. Rep. **8**(1), 7986 (2018).
23. A. Carpentier, M. Canney, A. Vignot, V. Reina, K. Beccaria, C. Horodyckid, C. Karachi, D. Leclercq, C. Lafon, J. Y. Chapelon, L. Capelle, P. Cornu, M. Sanson, K. Hoang-Xuan, J. Y. Delattre, and A. Idbaih, "Clinical trial of blood-brain barrier disruption by pulsed ultrasound," Sci. Transl. Med. **8**(343), 343re2 (2016).
24. N. Lipsman, S. Ironside, R. Alkins, A. Bethune, Y. Huang, J. Perry, A. Sahgal, M. Trudeau, K. Hynynen, and T. Mainprize, "SCDT-51. Initial experience of blood-brain barrier opening for chemotherapeutic-drug delivery to brain tumors by MR-guided focused ultrasound," Neuro-oncol. **19**(suppl_6), vi275 (2017).
25. C. C. Chen, P. S. Sheeran, S. Y. Wu, O. O. Olumolade, P. A. Dayton, and E. E. Konofagou, "Targeted drug delivery with focused ultrasound-induced blood-brain barrier opening using acoustically-activated nanodroplets," J. Control. Release **172**(3), 795–804 (2013).
26. S. Y. Wu, S. M. Fix, C. B. Arena, C. C. Chen, W. Zheng, O. O. Olumolade, V. Papadopoulou, A. Novell, P. A. Dayton, and E. E. Konofagou, "Focused ultrasound-facilitated brain drug delivery using optimized nanodroplets: vaporization efficiency dictates large molecular delivery," Phys. Med. Biol. **63**(3), 035002 (2018).
27. K. A. Hallam, E. M. Donnelly, A. B. Karpiouk, R. K. Hartman, and S. Y. Emelianov, "Laser-activated perfluorocarbon nanodroplets: a new tool for blood brain barrier opening," Biomed. Opt. Express **9**(9), 4527–4538 (2018).
28. P. S. Sheeran and P. A. Dayton, "Phase-change contrast agents for imaging and therapy," Curr. Pharm. Des. **18**(15), 2152–2165 (2012).
29. K. Wilson, K. Homan, and S. Emelianov, "Biomedical photoacoustics beyond thermal expansion using triggered nanodroplet vaporization for contrast-enhanced imaging," Nat. Commun. **3**(1), 618 (2012).
30. E. Strohm, M. Rui, I. Gorelikov, N. Matsuura, and M. Kolios, "Vaporization of perfluorocarbon droplets using optical irradiation," Biomed. Opt. Express **2**(6), 1432–1442 (2011).
31. A. S. Hannah, G. P. Luke, and S. Y. Emelianov, "Blinking Phase-Change Nanocapsules Enable Background-Free Ultrasound Imaging," Theranostics **6**(11), 1866–1876 (2016).
32. G. P. Luke, A. S. Hannah, and S. Y. Emelianov, "Super-Resolution Ultrasound Imaging in Vivo with Transient Laser-Activated Nanodroplets," Nano Lett. **16**(4), 2556–2559 (2016).
33. H. Yoon, S. K. Yarmoska, A. S. Hannah, C. Yoon, K. A. Hallam, and S. Y. Emelianov, "Contrast-enhanced ultrasound imaging in vivo with laser-activated nanodroplets," Med. Phys. **44**(7), 3444–3449 (2017).
34. H. Yoon, K. A. Hallam, C. Yoon, and S. Y. Emelianov, "Super-resolution imaging with ultrafast ultrasound imaging of optically triggered perfluorohexane nanodroplets," IEEE Trans. Ultrason. Ferroelectr. Freq. Control **65**(12), 2277–2285 (2018).

Biomedical Optics EXPRESS

35. A. Hannah, G. Luke, K. Wilson, K. Homan, and S. Emelianov, "Indocyanine green-loaded photoacoustic nanodroplets: dual contrast nanoconstructs for enhanced photoacoustic and ultrasound imaging," ACS Nano **8**(1), 250–259 (2014).
36. A. S. Hannah, D. VanderLaan, Y. S. Chen, and S. Y. Emelianov, "Photoacoustic and ultrasound imaging using dual contrast perfluorocarbon nanodroplets triggered by laser pulses at 1064 nm," Biomed. Opt. Express **5**(9), 3042–3052 (2014).
37. D. Y. Santiesteban, D. S. Dumani, D. Profili, and S. Y. Emelianov, "Copper Sulfide Perfluorocarbon Nanodroplets as Clinically Relevant Photoacoustic/Ultrasound Imaging Agents," Nano Lett. **17**(10), 5984–5989 (2017).
38. P. S. Sheeran, N. Matsuura, M. A. Borden, R. Williams, T. O. Matsunaga, P. N. Burns, and P. A. Dayton, "Methods of Generating Submicrometer Phase-Shift Perfluorocarbon Droplets for Applications in Medical Ultrasonography," IEEE Trans. Ultrason. Ferroelectr. Freq. Control **64**(1), 252–263 (2017).
39. D. Y. Santiesteban, K. A. Hallam, S. K. Yarmoska, and S. Y. Emelianov, "Color-coded perfluorocarbon nanodroplets for multiplexed ultrasound and photoacoustic imaging," Nano Res. **12**(4), 741–747 (2019).
40. N. Rapoport, "Drug-Loaded Perfluorocarbon Nanodroplets for Ultrasound-Mediated Drug Delivery," Adv. Exp. Med. Biol. **880**, 221–241 (2016).
41. S. K. Yarmoska, H. Yoon, and S. Y. Emelianov, "Lipid Shell Composition Plays a Critical Role in the Stable Size Reduction of Perfluorocarbon Nanodroplets," Ultrasound Med. Biol. **45**(6), 1489–1499 (2019).
42. D. S. Li, S. Schneewind, M. Bruce, Z. Khaing, M. O'Donnell, and L. Pozzo, "Spontaneous Nucleation of Stable Perfluorocarbon Emulsions for Ultrasound Contrast Agents," Nano Lett. **19**(1), 173–181 (2019).
43. S. L. Jacques, "Optical properties of biological tissues: a review," Phys. Med. Biol. **58**(11), R37–R61 (2013).
44. H. M. Grey, J. W. Hirst, and M. Cohn, "A new mouse immunoglobulin: IgG3," J. Exp. Med. **133**(2), 289–304 (1971).
45. R. K. Hartman, K. A. Hallam, E. M. Donnelly, and S. Y. Emelianov, "Photoacoustic imaging of gold nanorods in the brain delivered via microbubble-assisted focused ultrasound: a tool for *in vivo* molecular neuroimaging," Laser Phys. Lett. **16**(2), 025603 (2019).
46. P. H. Wang, H. L. Liu, P. H. Hsu, C. Y. Lin, C. R. Wang, P. Y. Chen, K. C. Wei, T. C. Yen, and M. L. Li, "Gold-nanorod contrast-enhanced photoacoustic micro-imaging of focused-ultrasound induced blood-brain-barrier opening in a rat model," J. Biomed. Opt. **17**(6), 061222 (2012).